MODELLING THE CORONAL MAGNETIC FIELD USING HINODE (AND FUTURE) DATA

M. S. WHEATLAND* and S. A. GILCHRIST

School of Physics,
Sydney Institute for Astrophysics,
University of Sydney,
NSW 2006, Australia
**E-mail: m.wheatland@physics.usyd.edu.au*
www.physics.usyd.edu.au/˜wheat

S. RÉGNIER

School of Mathematics and Statistics,
University of St Andrews,
St Andrews, Fife KY 16 9SS,
United Kingdom
E-mail: stephane@mcs.st-andrews.ac.uk

There is considerable interest in accurate modelling of the solar coronal magnetic field using photospheric vector magnetograms as boundary data, and the nonlinear force-free model is often used. However, recent studies using Hinode data have demonstrated that this modelling fails in basic ways, with the failure attributable to the departure of the inferred photospheric magnetic field from a force-free state. The solar boundary data are inconsistent with the model, which leads to inconsistencies in calculated force-free solutions. A method for constructing a self-consistent nonlinear force-free solution is described, which identifies a force-free solution that is close to the observed boundary data. Steps towards developing more sophisticated magneto-hydrostatic modelling – taking into account pressure and gravitational forces at the level of the solar boundary data – are also outlined.

Accepted for publication in Advances in Geosciences (World Scientific: Singapore).

Acceptance date: 26 Nov 2009.

1. Background

1.1. *Coronal magnetic field modelling*

Solar flares are large magnetic explosions in the Sun's corona, powered by intense active region magnetic fields around sunspots.[17] Large flares influence our local space weather, including producing energetic particle storms which can damage satellite electronics. It has been estimated that a space weather 'superstorm' at the next solar maximum could produce an economic loss of up to \$70 billion[16] due to lost revenue and infrastructure. Space weather effects provide a motivation for developing accurate modelling of solar coronal magnetic fields, with the aim of better understanding and predicting large-scale solar activity.

Spectro-polarimetric measurements of certain photospheric lines permit a determination of the vector magnetic field at the photosphere. The resulting vector magnetograms are inferences rather than direct measurements,[4] and involve a number of uncertainties, but they provide the most detailed available information about active region magnetic fields. A new generation of instruments, including the spectropolarimeter (SP) of the Solar Optical Telescope (SOT) on the Hinode satellite,[23] is producing state-of-the-art data. In principle vector magnetograph data provides a set of boundary values for modelling the overlying coronal field, but in practice basic difficulties prevent the construction of reliable models from the data.[5,22]

1.2. *The nonlinear force-free model*

The nonlinear force-free model, involving a static balance of purely magnetic forces, is often used to describe the coronal magnetic field in the low density solar corona.[6,12,20] A nonlinear magnetic field $\mathbf{B}$ satisfies

$$\mathbf{J} \times \mathbf{B} = 0 \qquad \text{and} \qquad \nabla \cdot \mathbf{B} = 0, \tag{1}$$

where $\mathbf{J} = \mu_0^{-1} \nabla \times \mathbf{B}$ is the electric current density. The first of Eqs. (1) states that $\mathbf{J}$ is everywhere parallel to the magnetic field, and hence the equations may be reformulated as:

$$\nabla \times \mathbf{B} = \alpha \mathbf{B} \tag{2}$$

$$\mathbf{B} \cdot \nabla \alpha = 0, \tag{3}$$

introducing the force-free parameter α. Eq. (3) states that that α is constant along magnetic field lines.

The boundary conditions for the problem comprise a specification of the normal component of $\mathbf{B}$ in the boundary (denoted B_n), together with a specification of α over one polarity (sign) of B_n.[1,3,7,20] Equivalently, the boundary condition on α may be replaced by a specification of the normal component J_n of the electric current density over one polarity of B_n. We label the two choices of polarity as P (corresponding to $B_n > 0$), and N (corresponding to $B_n < 0$). It is only necessary to specify the force-free parameter (or J_n) on one polarity because of the constancy of α along field lines in the model.

In application to vector magnetograph data, boundary values for α may be constructed via finite differencing of the vector magnetogram values $B_x^{\rm vm}$ and $B_y^{\rm vm}$ parallel to the surface, according to

$$\alpha^{\rm vm} = \frac{1}{B_z^{\rm vm}} \left(\frac{\partial B_y^{\rm vm}}{\partial x} - \frac{\partial B_x^{\rm vm}}{\partial y} \right). \tag{4}$$

In the modelling described here solar curvature is ignored, and the boundary field values are assumed to lie in the plane $z = 0$. If Eq. (4) is applied over the observed vector magnetogram region it provides two possible choices for boundary values on α, corresponding to the P and N choices.

The nonlinear force-free equations are difficult to solve in the general 3-D case. A variety of iterative numerical methods have been developed,[28] and demonstrated to work on theoretical test cases.[21] Some of the methods use the specification of the full vector field in the boundary as boundary conditions, rather than the boundary conditions outlined above. This is formally an over-prescription, but should not introduce a problem if the boundary values are consistent with the force-free model.

The current-field iteration, or Grad-Rubin,[7] method provides one numerical approach to solving the nonlinear force-free model. This method involves solution, at iteration k, of the scheme:

$$\mathbf{B}^{[k]} \cdot \nabla \alpha^{[k+1]} = 0, \tag{5}$$

$$\nabla \times \mathbf{B}^{[k+1]} = \alpha^{[k+1]} \mathbf{B}^{[k]}. \tag{6}$$

If $\mathbf{B}^{[k]}$ is known then Eq. (5) is a linear equation for $\alpha^{[k+1]}$, allowing propagation of boundary values of the force-free parameter into the volume. The right-hand side of Eq. (6) is then known, and it is also a linear equation (Ampère's law) for $\mathbf{B}^{[k+1]}$, which may be solved in the volume subject to the boundary conditions on the field.

A fixed point of the iteration, $\mathbf{B} = \mathbf{B}^{[k+1]} = \mathbf{B}^{[k]}$, is a solution of the nonlinear Eqs. (2) and (3). There are a number of specific implementations of this method, involving different methods of solution of the equations, and different ways of imposing the boundary conditions.[2,3,25] Typically the scheme is started with from the potential field $\mathbf{B}^{[0]} = \mathbf{B}_{\rm pot}$ satisfying the boundary values of B_z. All Grad-Rubin methods use the mathematically correct boundary conditions on α specified above.

A fast current-field iteration implementation was presented in Ref. 25, namely a method with a computational time which scales as N^4, for a grid with N^3 points. Eq. (5) is solved by field line tracing such that $\nabla \cdot \mathbf{J}^{[k]} = 0$ is enforced, and Eq. (6) is solved using 2-D Fourier Transforms and a vector potential, thereby ensuring $\nabla \cdot \mathbf{B}^{[k]} = 0$.

1.3. *The failure of the nonlinear force-free model*

Two recent workshops have applied nonlinear force-free modelling to Hinode SOT/SP data.[5,22] A workshop in 2007 used data for NOAA active region AR 10930, observed on 12-13 December 2006, and a workshop in 2008 used data for AR 10953, observed on 30 April 2007. The workshops found that the force-free methods fail in basic ways in application to the solar data. Different methods produce solutions which are inconsistent with one another. For example, the estimates of magnetic free energy for AR 10930 varied between 1% and 32% of the energy $E_{\rm p}$ of the potential field with the same boundary values $B_z^{\rm vm}$, for solutions using different methods of solution of the force-free model but based on the same 'preprocessed' boundary data (this procedure is discussed below).[22] The solutions produced by individual methods are also not *self-consistent*. For example, for AR 10953, the P and N solutions produced by the fast current-field iteration method[25] had free magnetic energies equal to 3% and 18% of $E_{\rm p}$ respectively.[5]

The left-hand panel of Figure 1 illustrates the inconsistency. This shows the field lines for the P solution (dark lines) and the N solution (light lines) for AR 10953, for the central part of the active region, in a view looking directly down on the computational domain. The field lines are qualitatively very dissimilar, and the light field lines are clearly more twisted, reflecting the fact that this solution has larger values of $|\alpha|$, and a correspondingly greater free energy. Despite this basic inconsistency, nonlinear force-free modelling continues to be applied to solar boundary data. Caveat emptor![a]

The failure of the model may be attributed to the departure of the vector magnetogram field values from a force-free state. Errors in the field determination may contribute, but it is generally believed that the photospheric field is subject to non-magnetic forces.[13] The net force and torque on the coronal magnetic field may be evaluated via surface integrals of the boundary field values, which provide necessary conditions for consistency of the boundary data with the force-free model.[15] These integrals are typically significantly non-zero for vector magnetogram data.

[a]Let the buyer beware!

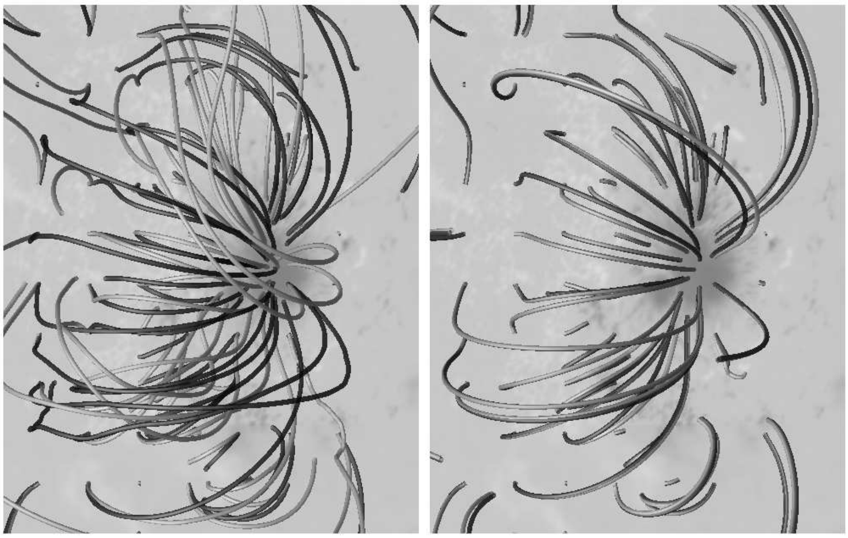

Fig. 1. Nonlinear force-free magnetic field solutions for AR 10953, constructed using the fast current-field iteration method applied to Hinode SOT/SP data. The field lines for the solutions are shown for the central part of the active region, in a view looking down on the computational domain. Left panel: The P (dark field lines) and N (light field lines) solutions obtained from the original data – these solutions use the boundary values for the force-free parameter on the positive and negative polarity respectively, and illustrate the inconsistency of the boundary data with the force-free model. Right panel: The P and N solutions after 10 self-consistency cycles.

One approach to the problem is 'preprocessing,' whereby the boundary data are modified so as to satisfy the necessary conditions.[29] Preprocessing of solar-like boundary data has shown to lead to improved nonlinear force-free solutions,[14] and preprocessing was applied to the data at the workshops in 2007 and 2008 in the modelling of ARs 10930 and 10953.[5,22] However, preprocessed solar photospheric vector magnetic field data *remains inconsistent with the force-free model*, as shown by the inconsistency of the P and N solutions in the left panel of Figure 1. The conditions being enforced are necessary but not sufficient, and there are an infinite number of such conditions.[1] Although preprocessing enforces some of these conditions, it does not enforce others, as shown explicitly in Ref 5 for the AR 10953 data (see Figure 5 in that paper). A further problem with preprocessing is that it typically involves smoothing the data, which is undesirable. The Hinode data are distinguished by its high resolution, and this should be exploited in modelling.

2. Self-consistent nonlinear force-free modelling

An alternative approach involves identifying a force-free solution which is, in some sense, close to the observed (non-force-free) boundary data. A specific method, in the context of the current-field iteration approach to solving the nonlinear force-free model, is presented in Ref 26, and is demonstrated in application to Hinode SOT/SP data for AR 10953.

2.1. *The self-consistency method*

There are three steps in the 'self-consistency' method.[26] First, the P and N solutions are constructed, from the (unpreprocessed) vector magnetogram boundary data. The vector magnetogram-derived boundary values of the force-free parameter are denoted by $\alpha_0 \pm \sigma_0$, where σ_0 are uncertainties calculated from the corresponding uncertainties in the inferred magnetic field values.[11] The P solution provides a mapping, along field lines, of boundary values at points in the region P to points in N, and thereby defines new possible boundary values $\alpha_1 \pm \sigma_1$ of the force-free parameter at points in N. Similarly, the N solution maps boundary values at points N to points in P, and so defines new possible boundary values $\alpha_1 \pm \sigma_1$ at points in N. Hence the two solutions define a complete new set of boundary values $\alpha_1 \pm \sigma_1$ (over both polarities).

Step two involves deciding on a new boundary value for α at each boundary point based on two possible choices $\alpha_0 \pm \sigma_0$ and $\alpha_1 \pm \sigma_1$. For this purpose Bayesian probability is applied.[8] The assumption of Gaussian errors and an application of Bayes's theorem lead to a most probable value, and associated uncertainty:[26]

$$\alpha_2 = \frac{\alpha_0/\sigma_0^2 + \alpha_1/\sigma_1^2}{1/\sigma_0^2 + 1/\sigma_1^2} \qquad \text{and} \qquad \sigma_2 = \left(\frac{1}{\sigma_0^2} + \frac{1}{\sigma_1^2}\right)^{-1/2}. \tag{7}$$

In other words, the new value is an uncertainty-weighted average of the two possible values. The new set of boundary values over all boundary points is still, in general, inconsistent with the force-free model, but the values are expected to be closer to consistency.

Step three involves iterating steps one and two. Two new force-free solutions are constructed for the P and N choices using the boundary values $\alpha_2 \pm \sigma_2$, via two separate applications of current-field iteration. Together, the two new solutions define new mappings between the P and N regions, and hence a complete new set of boundary conditions $\alpha_3 \pm \sigma_3$. Eqs. (7) are applied to $\alpha_2 \pm \sigma_2$ and $\alpha_3 \pm \sigma_3$ to decide on most probable values $\alpha_4 \pm \sigma_4$ at each boindary point, and so on.

Each iteration of the procedure [construction of the P and N solutions, and then application of Eqs. (7)] is referred to as a 'self-consistency cycle.' It is expected that the procedure converges to a self-consistent solution, i.e. a set of boundary values of the force-free parameter for which the P and N solutions are the same.

2.2. *Application to Hinode data*

In Ref. 26 the achievement of self-consistency is demonstrated using the Hinode SOT/SP data for AR 10953. The right-hand panel of Figure 1 illustrates the final, self-consistent solution, after 10 self-consistency cycles. The field lines for the P and N solutions, shown by dark and light lines respectively, agree closely. The energies for the two solutions differ by less than 0.03%.

The self-consistency procedure changes the boundary values. The changes are quite significant for the AR 10953 case, representing an rms change of about 120 G in B_x and about 100 G in B_y. This reflects the fairly gross discrepancies between the initial P and N solutions seen in the left panel of Figure 1. The changes are comparable to the changes introduced by preprocessing for the preprocessed data used at the workshop (preprocessing changes the B_z values also, whereas the B_z values are preserved in the self-consistency procedure).

It should be noted that the application to AR 10953 demonstrated in Ref 26 is at the level of a 'proof of concept' and could be improved in many ways. Uncertainties were not incorporated into the procedure (all points were assumed to have equal uncertainties). Also, the Hinode SOT/SP data used was embedded in a larger SOHO/MDI field of view for which only B_z values were available, and α was assigned to zero for this region. The rms changes introduced by the procedure are expected to be smaller once these limitations are removed. The calculation will be repeated including uncertainties and avoiding embedding in the near future.

3. Magneto-hydrostatic modelling

Whilst the self-consistency procedure outlined above provides one approach to constructing a coronal magnetic field model, and addresses the specific difficulty preventing the construction of a nonlinear force-free model, it is desirable to have a physical solution to the problem, i.e. an approach incorporating non-magnetic forces.

It is likely that the magnetic field at the photospheric level is subject to magnetic forces as well as pressure gradients, and dynamical forces (associated with flows). All of these forces are expected to be significant at the photospheric level and in at least a narrow layer above that level. However, here we consider the next simplest model, i.e. a static model incorporating pressure and magnetic forces, but neglecting gravity, referred to as the magneto-hydrostatic (MHS) model. The MHS equations may be written:

$$\mathbf{J} \times \mathbf{B} = \nabla p \qquad \text{and} \qquad \nabla \cdot \mathbf{B} = 0, \tag{8}$$

where p is the gas pressure, the new dependent variable in the model.

Other forms of the equations are also useful. The first of Eqs. (8) implies

$$\mathbf{B} \cdot \nabla p = 0 \tag{9}$$

$$\mathbf{J} \cdot \nabla p = 0, \tag{10}$$

i.e. p is constant along field lines of $\mathbf{B}$ and stream lines of $\mathbf{J}$. It is convenient to separate $\mathbf{J}$ into components parallel and perpendicular to $\mathbf{B}$:

$$\mathbf{J} = \mathbf{J}_{\parallel} + \mathbf{J}_{\perp}, \tag{11}$$

with the parallel component represented in terms of a scalar function α:

$$\mathbf{J}_{\parallel} = \frac{1}{\mu_0} \alpha \mathbf{B}. \tag{12}$$

Setting $\nabla \cdot \mathbf{J} = 0$ leads to

$$\mathbf{B} \cdot \nabla \alpha + \mu_0 \nabla \cdot \mathbf{J}_{\perp} = 0, \tag{13}$$

and taking the cross product of $\mathbf{B}$ with the first of Eqs. (8) gives

$$\mathbf{J}_{\perp} = \frac{1}{B^2} \mathbf{B} \times \nabla p. \tag{14}$$

The boundary conditions for the problem comprise a specification of B_n together with a specification of J_n and p over one polarity of B_n.[7] The need to specify J_n and p over only one polarity follows from Eqs. (9) and (10).

3.1. *The Grad-Rubin method*

There have been relatively few attempts to solve the 3-D MHS equations from boundary conditions. One approach to solving the model in the solar context was presented in Ref 31 and Ref 32, and subsequently developed in spherical co-ordinates.[18,30] That approach is a generalisation of the optimisation method for calculating nonlinear force-free fields.[24,27] Here we consider a different method, a generalisation of current-field iteration, based on a qualitative description given in Grad and Rubin in Ref. 7.

The Grad-Rubin iteration scheme for the MHS problem may be summarised as:

$$\mathbf{B}^{[k]} \cdot \nabla p^{[k+1]} = 0 \tag{15}$$

$$\mathbf{J}_{\perp}^{[k+1]} = \mathbf{B}^{[k]} \times \nabla p^{[k+1]}/(B^{[k]})^2, \tag{16}$$

$$\mathbf{B}^{[k]} \cdot \nabla \alpha^{[k+1]} = -\mu_0 \nabla \cdot \mathbf{J}_{\perp}^{[k+1]}, \tag{17}$$

$$\nabla \times \mathbf{B}^{[k+1]} = \alpha^{[k+1]}\mathbf{B}^{[k]} + \mu_0 \mathbf{J}_{\perp}^{[k+1]}. \tag{18}$$

If $\mathbf{B}^{[k]}$ is known then Eq. (15) is a linear equation for $p^{[k+1]}$, allowing propagation of boundary values of pressure into the volume. Eq. (16) then allows the calculation of the perpendicular component of the current density $\mathbf{J}_{\perp}^{[k+1]}$ in the volume and on the boundary. Given those values, Eq. (17) is a linear equation for $\alpha^{[k+1]}$ allowing propagation of boundary values of the scalar function $\alpha^{[k+1]}$ into the volume. [The boundary values of $\alpha^{[k+1]}$ need to be constructed from the boundary values of J_n and the calculated boundary values of $\mathbf{J}_{\perp}^{[k+1]}$ at the given iteration, according to Eqs. (11) and (12).] The right-hand side of Eq. (18) is then known in the volume, and this equation is a linear equation for $\mathbf{B}^{[k+1]}$ (Ampère's law), which may be solved in the volume subject to the boundary conditions on the field. The scheme may be started from the potential field $\mathbf{B}^{[0]} = \mathbf{B}_{\rm pot}$ satisfying the boundary values of B_z. A fixed point of the iteration is a solution of the nonlinear problem.

A code implementing a method of solution of the iteration scheme (15)–(18) is currently being developed and tested. The code uses techniques similar to those used in the fast current-field iteration code for the nonlinear force-free problem.[25] Full details of the code and methods, and initial results for a simple test case will be given in a later publication.

3.2. *Prospects for application to data*

In principle spectro-polarimetric data provides not just magnetic, but also thermodynamic information, so that it is possible to infer plasma parameters from the observations.[9,10] Typically the thermodynamic parameters are ignored, in standard 'inversion' procedures. However, methods have been developed for reliable extraction of additional information, including the pressure profile in the atmosphere.[4,19] In principle this data provides additional boundary information for coronal field modelling.

In practice it may be necessary to introduce gravity into the magnetohydrostatic modelling, to make the atmospheric model more realistic. This requires an additional dependent variable, density, but with the assumption of an equation of state the density is simply related to pressure. The Grad-Rubin scheme may also be applied in this case. However, prospects for modelling from the data remain to be investigated in detail.

4. Summary

In principle, photospheric vector magnetogram data provides boundary data for coronal magnetic field modelling, and state-of-the-art data are being returned by new instruments including the SOT/SP on the Hinode spacecraft. In practice, however, modelling has proved difficult.

The nonlinear force-free model is appropriate in the corona, but it does not describe the field at the photospheric level, corresponding to the solar data. The model is inconsistent with the data, and this has lead to a failure of nonlinear force-free modelling.[5,22] Preprocessing the data to make it more compatible with the model[29] does not solve the inconsistency problem.

An approach to identifying a 'self-consistent' nonlinear force-free solution, which has boundary values close to the observed data, is described.[26] This provides one possible avenue for successful modelling. An alternative is to consider more sophisticated physical models, incorporating non-magnetic forces. A method for solving the magneto-hydrostatic (MHS) equations using Grad-Rubin iteration[7] is briefly described. A code implementing this method is currently being developed.

Acknowledgments

Stephane Régnier acknowledges the support of a Royal Society Short Visit Grant during a visit to the University of Sydney.

References

1. J. J. Aly, *Solar Phys.* **120**, 19 (1989).
2. T. Amari, J. J. Aly, J. F. Luciani, T. Z. Boulmezaoud and Z. Mikic 1997, *Solar Phys.* **174**, 129 (1997)
3. T. Amari, T. Z. Boulmezaoud, and J. J. Aly, *Astron. Astrophys.* **446**, 691 (2006).
4. J. C. Del Toro Iniesta and B. Ruiz Cobo, *Solar Phys.* **164**, 169 (1996).
5. M. L. DeRosa, C. J. Schrijver, G. Barnes, K. D. Leka, B. W. Lites, M. J. Aschwanden, T. Amari, A. Canou, J. M. McTiernan, S. Régnier, J. K. Thalmann, G. Valori, M. S. Wheatland, T. Wiegelmann, M. C. M. Cheung, P. A. Conlon, M. Fuhrmann, B. Inhester and T. Tadesse, *Astrophys. J.* **696**, 1780 (2009).
6. G. A. Gary, *Solar Phys.* **203**, 71 (2001).

7. H. Grad and H. Rubin, in *Proc. 2nd Int. Conf. on Peaceful Uses of Atomic Energy*, Vol. 31, United Nations, Geneva (1958), p. 190.
8. E. T. Jaynes, *Probability Theory*, ed. G. Larry Bretthorst, Cambridge University Press, Cambridge, UK (2003).
9. J. Jefferies, B. W. Lites and A. Skumanich, *Astrophys. J.* **343**, 920 (1989).
10. E. Landi Degl'Innocenti and M. Landolfi, *Polarization in Spectral Lines*, Dordrecht, Kluwer (2004).
11. K. D. Leka and A. Skumanich, *Solar Phys.* **188**, 3 (1999).
12. A. N. McClymont, L. Jiao, and Z. Mikic, *Solar Phys.* **174**, 191 (1997).
13. T. R. Metcalf, L. Jiao, A. N. McClymont, R. C. Canfield and H. Uitenbroek, *Solar Phys.* **247**, 269 (1995).
14. T. R. Metcalf, M. L. Derosa, C. J. Schrijver, G. Barnes, G., A. A. van Ballegooijen, T. Wiegelmann, T., M. S. Wheatland, G. Valori and J. M. McTtiernan, *Solar Phys.* **247**, 269 (2008).
15. M. M. Molodenskii, *Sov. Astron.* **12**, 585 (1969).
16. S. Odenwald, J. Green, and W. Taylor, *Adv. Sp. Res.* **38**, 280 (2006).
17. E. R. Priest and T. G. Forbes, *Astron. Astrophys. Rev.* **10**, 313 (2002).
18. P. Ruan, T. Wiegelmann, B. Inhester, T. Neukirch, S. K. Solanki and L. Feng, *Astron. Astroph.* **481**, 827 (2008).
19. B. Ruiz Cobo and J. C. del Toro Iniesta, *Astrophys. J.*, **398**, 375 (1992).
20. T. Sakurai, *Solar Phys.* **69**, 343 (1981).
21. C. J. Schrijver, M. L. Derosa, T. R. Metcalf, Y. Liu, J. McTiernan, S. Régnier, M. S. Wheatland and T. Wiegelmann, *Solar Phys.* **235**, 161 (2006).
22. C. J. Schrijver, M. L. DeRosa, T. Metcalf, G. Barnes, B. Lites, T. Tarbell, J. McTiernan, G. Valori, T. Wiegelmann, M. S. Wheatland, T. Amari, G. Aulanier, P. Demoulin, M. Fuhrmann, K. Kusano, S. Régnier and J. K. Thalmann, *Astrophys. J.* **675**, 1637 (2008).
23. S. Tsuneta, K. Ichimoto, Y. Katsukawa, S. Nagata, M. Otsubo, T. Shimizu, Y. Suematsu, M. Nakagiri, M. Noguchi, T. Tarbell, A. Title, R. Shine, W. Rosenberg, C. Hoffmann, B. Jurcevich, G. Kushner, M. Levay, B. Lites, D. Elmore, T. Matsushita, N. Kawaguchi, H. Saito, I. Mikami, L. D. Hill and J. K. Owens, *Solar Phys.* **249**, 167 (2008).
24. M. S. Wheatland, P. A. Sturrock and G. Roumeliotis, G. 2000, *Astrophys. J.* **540**, 1150 (2000).
25. M. S. Wheatland, *Solar Phys.* **245**, 251 (2007).
26. M. S. Wheatland and S. Régnier, *Astrophys. J.* **700**, L88 (2009).
27. T. Wiegelmann, *Solar Phys.* **219**, 87 (2004)
28. T. Wiegelmann, *J. Geophys. Res. A* **113**, 3 (2008).
29. T. Wiegelmann, B. Inhester and T. Sakurai, *Solar Phys.* **233**, 215 (2006).
30. T. Wiegelmann, T. Neukirch, P. Ruan and B. Inhester, *Astron. Astroph.* **475**, 701 (2007).
31. T. Wiegelmann and B. Inhester, *Solar Phys.* **214**, 287 (2003).
32. T. Wiegelmann and T. Neukirch, *Astron. Astroph.* **457**, 1053 (2006).